Nanometer Order Separation Control of Large Working Area Nanogap Created by Cleavage of Single-Crystal Silicon Along {111} Planes Using a MEMS Device

AUTHOR(S):

Shimofuri, Masaki; Banerjee, Amit; Hirotani, Jun; Hirai, Yoshikazu; Tsuchiya, Toshiyuki

CITATION:

Shimofuri, Masaki ...[et al]. Nanometer Order Separation Control of Large Working Area Nanogap Created by Cleavage of Single-Crystal Silicon Along {111} Planes Using a MEMS Device. Journal of Microelectromechanical Systems 2023, 32(1): 67-73

ISSUE DATE:

2023-02

URL:

http://hdl.handle.net/2433/279084

JMEMS-2022-0073-OM

Nanometer order separation control of large working area nanogap created by cleavage of single-crystal silicon along {111} planes using a MEMS device

Masaki Shimofuri, Amit Banerjee,
Jun Hirotani, Yoshikazu Hirai, and Toshiyuki Tsuchiya, *Member, IEEE*

***Abstract*— Nanogaps with a large working area and a precisely controlled separation of about 1 to 20 nm has important applications in nano photonics, thermal management, power generation, chemical sensing, etc. However, an effective method of fabricating such nanogaps has not yet been established. In addition, it has been necessary to evaluate the dependence of physical characteristics of nanogaps on the separation, but it has been technically and economically difficult to develop such a system. In this study, we developed a MEMS device, which can produce nanogaps with a large area and parallel smooth surfaces by the (111) plane cleavage of a single crystal silicon beam and can change and measure the separation of nanogaps. Using this device, nanogap fabrication by cleavage and separation control were uninterruptedly carried out while maintaining the cleanliness of the gap surfaces in vacuum; a nanogap with a large smooth surface area of 30 μm^2 was successfully controlled in the range of 14 nm–1.5 μm. For a small separation of less than 100 nm, the control resolution was sufficiently high at 1 nm. This method is fully compatible with conventional fabrication technologies for not only MEMS but also other semiconductor devices and should contribute to the fabrication of devices that exhibit useful quantum effects with only minor modifications.**

***Index Terms*—Nanogap, Casimir force, Van der Waals force, Lifshitz force, Thermophotovoltaic energy conversion (TPV), Thermionic energy conversion (TIC), Thermal nanotechnology**

I. Introduction

When the gap between two objects becomes nanometer-scale, phenomena different from those in the bulk appear owing to local electric field enhancement and quantum tunneling [1,2]. The phenomena occurring in the nanogap, such as, charge tunneling [1,3–5], near-field radiation [6,7], optical rectification [8], localized surface plasmon [8–10], and Casimir–van der Waals force [11], are not only important from the viewpoint of physics, but also have a wide range of applications, including in chemical and biosensors, such as, gas sensors [12] and SERS [2,8–10], in electronics, such as, vacuum transistors [3,4] and resistance switches [5], in thermal management technologies, such as, thermal diodes [7] and electronic refrigeration [13], and in highly efficient power generation, such as, thermophotovoltaic (TPV) energy conversion [14] and thermionic energy conversion (TIC) [13,15].

Nanogap fabrication has been studied for various materials, gap distances, and surface geometries, and various methods, such as, electron-beam lithography, electromigration [1,2], and ion beam technology [16] have been investigated. However, nanogaps with a narrow separation of about 1 to 20 nm fabricated by those methods usually have a very small working area. Therefore, these fabrication methods are not suitable for applications, such as, in thermal management and power generation, which require nanogaps with both small separations and large working areas. Moreover, although quantum phenomena between nanogaps have a strong dependence on the separation, the separation is less reproducible and fixed in most cases, and it is still difficult to change the separation or obtain a specific separation with high accuracy.

In a recent study of large-area nanogaps with controllable separation, Song et al. fabricated parallel-plate nanogaps made of SiO_2–SiO_2, Au–Au, SiO_2–Au, an Au–Si with a facing area of 40 × 40 μm^2 [17]. The separation was precisely controlled using a nano-positioner, and the near-field radiation characteristic was measured. The obtained separation was limited to 50 nm–10 μm because of cleanliness issues of the facing surfaces. Fiorino et al. fabricated parallel plate nanogaps with a microfabricated thermal emitter and a microscale solar cell [18]. They had a facing area of Φ80 μm, and their TPV power generation performance was evaluated by controlling the separation using a nano-positioner. However, the obtained separation was limited to 60 nm–12 μm for the same reason. To realize ultra-narrow gaps with a large working area, low surface roughness, high flatness, and high cleanliness are required over all the facing surfaces; there is still no method of fabricating large-area nanogaps of μm^2–mm^2 order with a separation of about 1 to 20 nm.

To fabricate nanogaps with a large working area and a controllable separation of about 1 to 20 nm, we have proposed a method of cleavage along the {111} crystal plane of a single-

This paragraph of the first footnote will contain the date on which you submitted your paper for review, which is populated by IEEE. This research was carried out with the support of JSPS KAKENHI Grant Number JP21H01261, the Yazaki Memorial Foundation for Science and Technology, Mori Manufacturing Research and Technology Foundation, and the Nanotechnology Platform Project in Kyoto.

Masaki Shimofuri, Amit Banerjee, Jun Hirotani, Yoshikazu Hirai, and Toshiyuki Tsuchiya is with Kyoto University, Kyoto 615-8540 Japan. (e-mail: m_shimofuri@nms.me.kyoto-u.ac.jp; banerjee.amit.3v@kyoto-u.ac.jp; hirotani@nms.me.kyoto-u.ac.jp; hirai@me.kyoto-u.ac.jp; tutti@me.kyoto-u.ac.jp)

crystal silicon (SCS) beam patterned on a MEMS device. This method yields nanogaps with large-area facing surfaces of 10–50 of μm^2 with a roughness in nm order, whose separation is less than 15 nm and can be varied and measured by MEMS. Furthermore, the process from gap fabrication by cleavage to separation control can be performed continuously in a vacuum environment by using an electrical control system. Therefore, the cleanliness of the gap surfaces, which had been an issue in previous research, can be maintained at a high level by preventing oxidation and contamination. We have previously reported on the observation of a pull-in phenomenon in nanogaps using this device and that pull-in was considered to be because of Lifshitz force [19]. In this paper, the measurement results are further analyzed by fitting a physical model and discussed in detail by considering both electrostatic forces and Lifshitz forces acting between the electrodes of the nanogap. We also discuss the validity of the proposed MEMS-based large-working-area nanogap fabrication method by evaluating the smoothness of the surfaces of the nanogap by high-resolution visual examination using a Field Emission Scanning Electron Microscopy (FE-SEM).

II. Method

A. MEMS device

The schematic diagram of the MEMS device is shown in Fig. 1. The fork-shaped shuttle of the device is supported by only two pairs of suspensions, and its central part is connected to a fixed anchor via a notch. When tensile force is applied to the shuttle, cleavage occurs at the notch and a gap is formed between the shuttle and the anchor. To minimize the displacement of the shuttle other than along the long axis direction, the part called “tab”, where the tensile force is applied, consists of all silicon-on-insulator (SOI) layers to increase rigidity. The tensile force is transmitted to the shuttle via hooks between the shuttle and the tab. A pin inserted into a hole of the tab is used to apply tensile force; however, it does not affect the accuracy of controlling the separation because the shuttle and the tab are separated by hooks except during gap fabrication. A stopper structure is patterned near the hook structure with a gap of 1.5 μm from the fixed part to prevent damage to the structure by the large displacement of the shuttle at the time of cleavage. After gap fabrication, the shuttle is driven in the long axis direction by comb electrostatic actuators on both sides to change the separation. All processes from applying the tensile force to controlling the separation can be operated remotely so that they can be performed inside the vacuum chamber of an SEM.

B. Nanogap fabrication by cleavage

In this study, we apply SCS cleavage to obtain nanogaps with large-area smooth surfaces suitable for various applications. SCS is a typical brittle material at room temperature and is known to fracture preferentially along the crystal planes of {111} and {110}. It has been reported that cleavage along the (110) plane deflects onto to the (111) plane because of bond

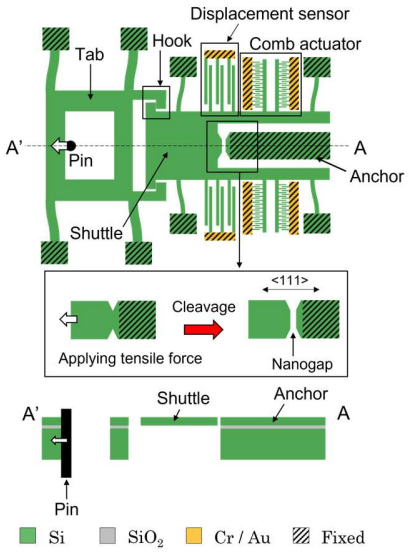

Fig. 1. Schematic diagram of MEMS device.

reconstruction near the crack tip [20], making it unstable and unsuitable for obtaining nanogaps with large-area smooth surfaces. On the other hand, cleavage along the (111) plane is not disrupted by deflection and produces smooth surfaces, as reported by the Uesugi et al. [21] Therefore, cleavage along the {111} plane is adopted in this study. This can be achieved by using (110) oriented silicon wafers because (111) plane exists in the direction orthogonal to (110) planes.

The design of the notches, which is the starting point of fracture, requires careful consideration to obtain smooth and straight surfaces. The symmetry of the notches on the left and right sides may initiate cracks from both sides at the same time, causing steps in the fracture surfaces. Therefore, notches on the left and right sides have different curvatures. Other features, such as, the shape and arrangement of etching holes, are made symmetrical, because the asymmetry of the structure near the notches can cause asymmetry in the stress field, which leads to crack deflection.

C. Separation control

To control the separation, the shuttle is driven by comb-drive actuators and the displacement of the shuttle is measured by parallel-plate capacitive sensor. The driving force of the comb-drive actuator shown in Fig. 2 is given by

$$F = \frac{1}{2}\frac{n_c \varepsilon_0 H}{g_c} V_c^2, \quad (1)$$

where n_c is the number of gaps of the comb actuator, ε_0 is the vacuum permittivity, H is the height of the structure (5 μm), and g_c is the separation between the comb teeth. The driving force does not depend on the displacement, and since there is almost no hysteresis, control with high accuracy is possible.

The parallel-plate capacitive sensors have an asymmetrical structure on both sides of the shuttle, and the displacement of the shuttle is measured using the capacitance difference between the left and right sensors.

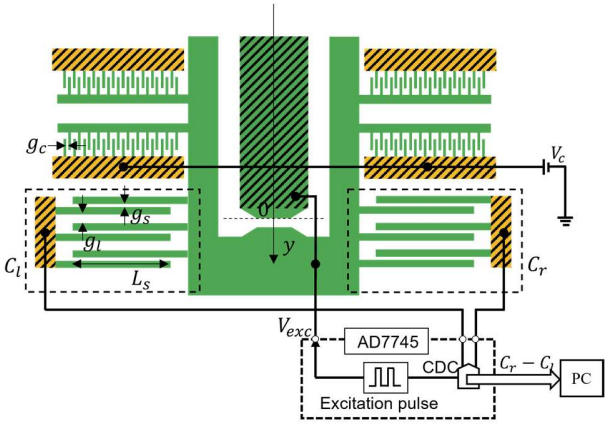

Fig. 2. Electric circuit for separation control.

$$C_l = \varepsilon_0 L_s H \left(\frac{n_s}{g_s - y} + \frac{n_l}{g_l + y} \right)$$
$$C_r = \varepsilon_0 L_s H \left(\frac{n_s}{g_s + y} + \frac{n_l}{g_l - y} \right) \quad (2)$$

When the displacement is sufficiently small, the capacitance difference can be approximated as eq. (4).

$$\Delta C = C_l - C_r \quad (3)$$
$$\approx 2\varepsilon_0 L_s H \left(\frac{n_s}{g_s^2} - \frac{n_l}{g_l^2} \right) y \quad (4)$$

The separation is controlled by the circuit shown in Fig. 2, and the capacitance-to-digital converter AD7745 is used to measure the capacitance difference. Excitation pulses of $0 - V_{exc}$ [V] are applied to the shuttle and the anchor, and the capacitance is measured by charging and discharging between the parallel plates of the sensors.

III. Experiments

A. Device fabrication

The MEMS device was fabricated from a SOI wafer with a 5-µm-thick device layer with (110) orientation, a 2-µm-thick buried oxide layer, and a 400-µm-thick handle layer. An overview of the fabrication process is given below and shown in Fig. 3.

(1) Resists for bilayer lift-off processing (PMGI SF5S) and a photoresist (TDMR-AR80) were spin-coated and patterned by photolithography using a stepper.
(2) Cr 50 nm, Au 200 nm (for electrodes), and Cr 50 nm (for a DRIE hard mask) thin-films were sequentially deposited by electron beam deposition and lifted off.
(3) A photoresist (TDMR-AR80) was spin-coated and patterned by photolithography using a stepper.
(4) Device layer structure was patterned by Deep Reactive Ion Etching (DRIE).
(5) A photoresist (CY1000) was spin-coated on the reverse side and patterned by contact photolithography using a mask/bond aligner.
(6) Handle layer structure was patterned by DRIE.
(7) Buried oxide layer was etched by vapor HF and the movable structure was released.

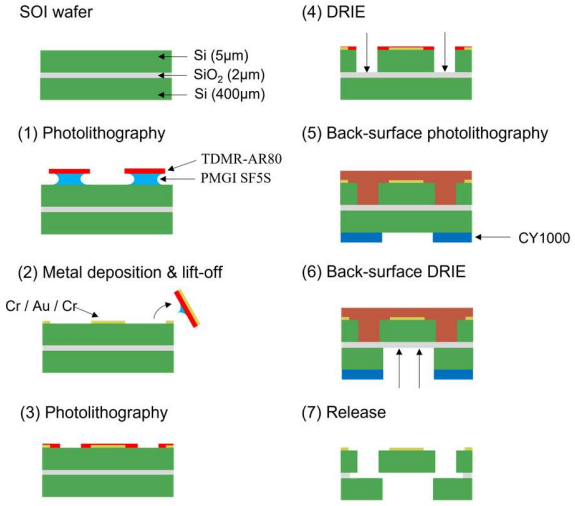

Fig. 3. Fabrication process flow.

B. Nanogap fabrication & gap control

A pin attached to a piezoelectric actuator was inserted into the hole of the tab of the device, and they were introduced into the vacuum chamber of SEM. Under SEM observation, a voltage was applied to the piezoelectric actuator, and a gap was formed by cleavage at the notches. After gap formation, the separation was changed by applying voltage to the comb-drive actuators while measuring the capacitance difference of sensors using the circuit shown in Fig. 2.

IV. Experimental Results

A. Fabrication result

SEM images of the fabricated device is shown in Fig. 4. The narrow pattern of the electrode was observed to be peeling up. This is considered to be due to tensile stress in the Cr layer. Fortunately, there was no warping of the shuttle, and no cracks were observed over the entire electrode, and voltage could be

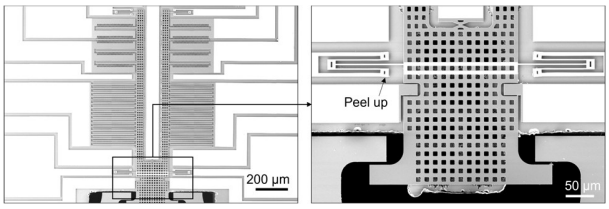

Fig. 4. SEM image of the fabricated device. [19]

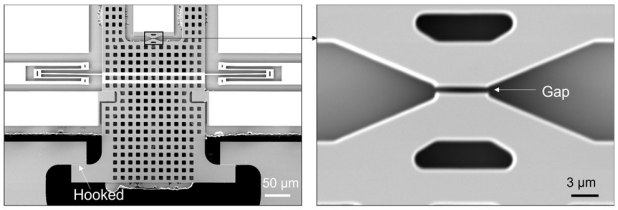

Fig. 5. SEM image of the device after gap formation. [19]

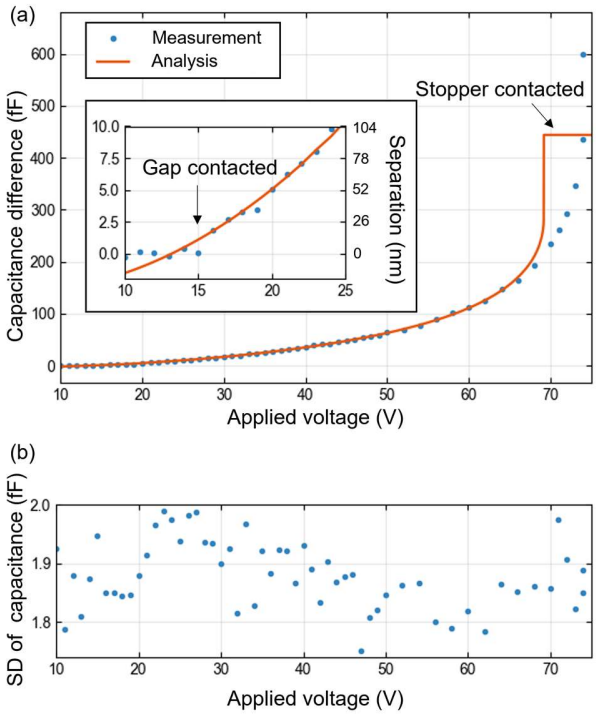

Fig. 6. Results of separation control in SEM. (a) Relationship between capacitance difference (fF) and applied voltage on comb actuator for gap widening. (b) Relationship between standard deviation of capacitance difference and applied voltage.

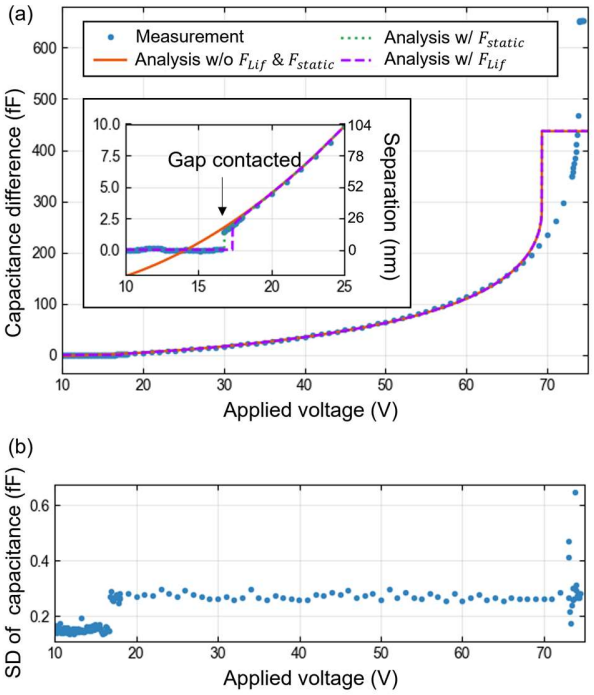

Fig. 7. Results of separation control in atmosphere. (a) Relationship between capacitance difference (fF) and applied voltage on comb actuator for gap widening. (b) Relationship between standard deviation of capacitance difference and applied voltage.

applied without any problem. Therefore, the effect of detachment on subsequent experiments, such as the accuracy of separation control, are considered to be small. The results of gap formation are shown in Fig. 5.

B. Nanogap fabrication & gap control

The displacement as a function of the voltage of the comb actuators for gap widening is shown in Fig. 6, where the voltage was decreased step by step from 74 V to 10 V. Above 75V, not only the stopper but also the teeth of the displacement sensor came into contact, so it was not included in the experiment. Almost no capacitance change was observed between 10 V and 15 V, indicating that gap contact occurred between 15 V and 16 V. The relationship between the displacement and the capacitance change was characterized by fitting the experimental results based on eq. (6) for the balancing of forces on the shuttle and eq. (3) for the relationship between the capacitance difference and the displacement (solid curve in Fig. 6(a)). For fitting, g_s and g_c, which are largely affected by the manufacturing error, are adopted as the fitting parameters, while the design values are used for the other parameters.

$$g = y + y_0, \tag{5}$$

$$F = -k_y g + \frac{1}{2}\frac{n_c \varepsilon_0 H}{g_c}\left(V_c^2 - V_c V_{exc} + \frac{1}{2}V_{exc}^2\right) + \frac{1}{2}\frac{V_{exc}^2}{2}\varepsilon_0 L_s H\left(\frac{n_s}{(g_s - g)^2} - \frac{n_l}{(g_l + g)^2}\right) - \frac{1}{2}\frac{V_{exc}^2}{2}\varepsilon_0 L_s H\left(\frac{n_s}{(g_s + g)^2} - \frac{n_l}{(g_l - g)^2}\right) = 0, \tag{6}$$

where g is the separation (unit is m), y_0 is a parameter used to correct the separation in the initial state, and k_y is the spring constant of the suspensions. Note that y_0 can take both positive and negative values. This is mainly due to residual stresses from the SOI wafer and internal stresses in the electrodes. The proportionality constant of 0.10 fF/nm was obtained for a sufficiently small separation of less than 100 nm.

Deviations from the experimental results were observed above 65 V, which may be caused by the deformation of the displacement sensor due to electrostatic forces and errors in the excitation voltage applied by AD7745 to the shuttle. This deviation at large separation has little effect on the fitting parameters, therefore the evaluation at small separation is expected to be reliable. A deviation was also observed at 10–15 V, which is considered to be due to pull-in caused by an attractive force acting within the gap. The effect of the attraction will be discussed in detail later. As shown in Fig. 6(b), the standard deviation (SD) of the measured capacitance ranged from 1.8 to 2.0 fF; therefore, we could not observe the small separation region in detail. In this measurement in vacuum, the

ground potential of the capacitance measurement and the ground potential of the SEM system were shared to prevent charging up during SEM observation, and the reason for the error in the measurement is considered to be the noise from the SEM system. Since displacement measurement and SEM observation are usually not necessary to be performed simultaneously, this problem can be solved by separating the ground potentials during displacement measurement.

Next, the same experiment was conducted in air without the effect of SEM system. The experimental results are shown in Fig. 7. The relationship between the separation and the capacitance change was calibrated by fitting the experimental results in the same way as that in the SEM (solid curve in Fig. 7(a)). For gaps sufficiently smaller than 100 nm, the proportionality constant of 0.10 fF/nm was obtained similarly to that in vacuum. The SD in capacitance measurement was about 0.3 fF (Fig. 7(b)), which corresponds to a measurement error of ±3 nm. The resolution of the separation control depends on the resolution of the applied voltage which is about 0.1 V and roughly corresponds to 1 nm displacement for in the small separation regime. Pull-in was clearly observed at 16.7 ± 0.1 V, where the minimum separation was 14 ± 3 nm.

C. Gap observation

The gap was observed from three directions using a FE-SEM system with high resolution. The images are shown in Figs. 8 and 9. The gap is closed because no voltage is applied to the actuator during observation. During fracture, the crack propagated in a straight-line except at the left and right edges, indicating that the gap surface is very smooth. The FE-SEM system has a resolution of about 1 nm; since no clear opening can be seen, the roughness of the gap surface is considered to be less than 1 nm.

V. Discussion

Here, the pull-in behavior of the nanogap is discussed. Forces such as Lifshitz force F_{Lif} and electrostatic force F_{static} act within gaps. Therefore, eq. (6) can be rewritten as

$$\begin{aligned} F = -k_y g + \frac{1}{2}\frac{n_c \varepsilon_0 H}{g_c}\left(V_c^2 - V_c V_{exc} + \frac{1}{2}V_{exc}^2\right) \\ + \frac{1}{2}\frac{V_{exc}^2}{2}\varepsilon_0 L_s H\left(\frac{n_s}{(g_s - g)^2} - \frac{n_l}{(g_l + g)^2}\right) \\ - \frac{1}{2}\frac{V_{exc}^2}{2}\varepsilon_0 L_s H\left(\frac{n_s}{(g_s + g)^2} - \frac{n_l}{(g_l - g)^2}\right) \\ + F_{Lif} + F_{static} = 0. \end{aligned} \tag{7}$$

Pull-in occurs when there is no stable equilibrium point y that satisfies eq. (7). The existence of a stable equilibrium point y is equivalent to the local maximum of F being greater than or equal to zero. Therefore, the minimum separation can be obtained by finding y where F takes a local maximum. Since the third and fourth terms can be ignored when the gap is small, the minimum separation can be obtained by solving

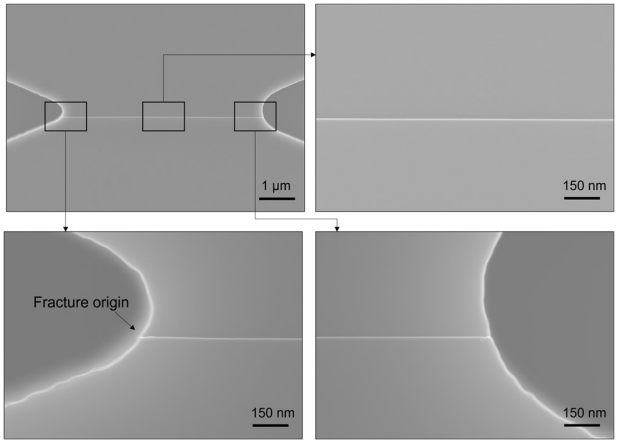

Fig. 8. FE-SEM images of top side.

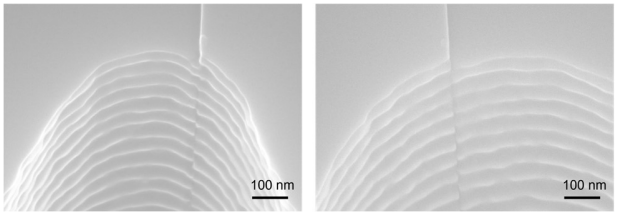

Fig. 9. FE-SEM images from left and right sides.

$$\frac{\partial F}{\partial g} = -k_y + \frac{\partial F_{Lif}}{\partial g} + \frac{\partial F_{static}}{\partial g} = 0. \tag{8}$$

(1) Electrostatic force
Local charging due to contact potential and tribo-charging occurs [22]. The electrostatic force is given by

$$F_{static} = -\frac{\varepsilon_0 A_{gap}}{g^2} V_{gap}^2, \tag{9}$$

where V_{gap} is the voltage acting between the gap and A_{gap} is the area of the gap. The dotted curve in Fig. 7 shows a numerical calculation assuming that the electrostatic force is dominant. A large potential of 0.2 V is required to match the experimental results.

(2) Lifshitz force
Casimir predicted the force between parallel plates made of conductors with gap d in a vacuum as

$$F_c = -\frac{\hbar c \pi^2 A_{gap}}{240 g^4}, \tag{10}$$

where c is the speed of light. This force is called Casimir force, which is due to the imbalance of the zero-point vibration mode inside and outside the gap [23]. Lifshitz proved that this force has the same origin as the van der Waals force and comprehended these forces to a theory that can be used for dielectric materials [24]. This is called Lifshitz force, which is given as

$$F_{Lif} = F_c \frac{120}{\pi^4} \sum_m \int_0^\infty dK\, K^3 \int_0^K \frac{d\Omega}{K} f(r_m^2, K, x)\,, \quad (11)$$

$$f(r_m^2, K, x) = \frac{r_m^2 (1 - e^{-2x})^2 e^{-2K}}{(1 - r_m^2 e^{-2x})^2 - r_m^2 (1 - e^{-2x})^2 e^{-2K}}, \quad (12)$$

$$r_p = \frac{\sqrt{K^2 + \Omega^2(\varepsilon - 1)} - \varepsilon K}{\sqrt{K^2 + \Omega^2(\varepsilon - 1)} + \varepsilon K}, \quad (13)$$

$$r_s = \frac{\sqrt{K^2 + \Omega^2(\varepsilon - 1)} - K}{\sqrt{K^2 + \Omega^2(\varepsilon - 1)} + K}, \quad (14)$$

$$\omega = i\xi, \quad (15)$$

$$\Omega = \frac{\xi g}{c} \quad (16)$$

$$x = \frac{w}{g}\sqrt{K^2 + \Omega^2(\varepsilon - 1)} \quad (17)$$

where $\varepsilon(\omega)$ and w are the dielectric function of the material and the thickness of plates, respectively [25]. Thus, the Lifshitz force can be calculated using the dielectric function of the material. For SCS, Duraffourg and Andreucci have calculated the Lifshitz force numerically for sufficiently thick plates and a doping level of 10^{18} cm^{-3} [25], and the following simple equation provides a good approximation for it.

$$F_{Lif} = \frac{0.33g}{g + 25.3 \times 10^{-9}} F_c \quad (18)$$

The dashed curve in Fig. 7(a) shows the results of numerical calculations considering the Lifshitz force. In the theoretical calculation, the separation at which pull-in occurs is about 17 nm, which is slightly different from the experimental result, but this is considered to be because of the fact that the temperature dependence was not taken into account in the calculation.

The shuttle and the anchor are electrically connected so that they are at the same potential, and the time constant is evaluated to be less than 10^{-11} [s]. Therefore, it is unlikely that electrostatic forces are dominant, and the pull-in observed is most likely due to the Lifshitz force. The relationship between the minimum separation and the spring constant of the suspensions can be derived from eqs. (8), (9), and (11). This allows the minimum separation to be predicted at the design phase of the fabrication process. When the electrostatic force is dominant, the minimum separation is given by

$$g_{min} = \sqrt[3]{\frac{2\varepsilon_0 A_{gap} V_{gap}^2}{k_y}}. \quad (19)$$

Thus, the minimum separation when electrostatic forces to be dominant is found to be proportional to the −1/3rd power of the spring constant of the suspensions. When the Lifshitz force is dominant, the approximation equation (18'), which holds when $g \ll 2.53$ nm, can be used to obtain the explicit form, eq. (20).

$$F_{Lif} = \frac{0.33g}{25.3 \times 10^{-9}} F_c \quad (18')$$

$$g_{min} = \sqrt[4]{\frac{\hbar c \pi^2 A_{gap}}{80 k_y} \frac{0.33}{25.3 \times 10^{-9}}} \quad (20)$$

Therefore, the minimum separation for Lifshitz forces being dominant is proportional to the −1/4th power of the spring constant of the suspensions. This means that as the gap becomes smaller, the Lifshitz force becomes more dominant than the electrostatic force. Particularly for a nanogap with a separation of less than 10 nm, the Lifshitz force becomes critically important. Thus, in the design of devices, the effect of the Lifshitz force must be considered.

VI. Conclusion

In this study, nanogaps with a large working area and parallel smooth surfaces were fabricated by the (111) plane cleavage of a SCS beam, whose separation can be changed and measured by MEMS. The experiments, from gap fabrication by cleavage to its separation control, were carried out continuously in vacuum, and nanogaps with large smooth surfaces of 30 μm^2 were obtained and their separation was successfully controlled in the range of 14 nm to 1.5 μm. For small separations of less than 100 nm, the resolution of separation control was estimated to be 1 nm, which has a sufficient resolution. The fabricated nanogap has extremely smooth surfaces, and the surface roughness was estimated to be less than 1 nm by FE-SEM observation. The proposed method is fully compatible with conventional fabrication methods for MEMS and other semiconductor devices. Compared with conventional methods for fabricating nanogaps [1,2, 16-18], it succeeds in achieving both a narrow gap and large working area, and additionally enables separation control at high resolution on the chip scale. In addition, the application of voltage or measuring temperature differences across gaps can be realized by simple design modifications, such as, by addition of electrodes, and our devices can be readily extended as tools for studying separation dependent phenomena specific to nanogaps.

References

[1] T. Li, W. Hu, and D. Zhu, "Nanogap Electrodes," *Adv. Mater.,* vol. 22, no. 2, pp. 286–300, Jan. 2009, doi: 10.1002/adma.200900864.
[2] Y. Yang, C. Gu, and J. Li, "Sub-5 nm Metal Nanogaps: Physical Properties, Fabrication Methods, and Device Applications," *Small*, vol. 15, no. 5, Feb. 2019, Art. no. 1804177, doi: 10.1002/smll.201804177.
[3] J.-W. Han, J. S. Oh and M. Meyyappan, "Vacuum Nanoelectronics: Back to the Future? —Gate Insulated Nanoscale Vacuum Channel Transistor," *Appl. Phys. Lett.*, vol. 100, no. 21, May 2012, Art. no. 213505, doi: 10.1063/1.4717751.
[4] S. Nirantar et al., "Metal−Air Transistors: Semiconductor-Free Field-Emission Air-Channel Nanoelectronics," *Nano Lett.*, vol. 18, no. 12, pp. 7478–7484, Nov 2012, doi: 10.1021/acs.nanolett.8b02849.
[5] J.-M. Nam, J.-W. Oh, H. Lee, and Y. D. Suh, "Resistance switch employing a simple metal nanogap junction," *Nanotechnology*, vol. 17, Oct. 2006, Art. no. 213505, doi: 10.1088/0957-4484/17/22/022.

[6] A. Didari, E. B. Elçioğlu, T. Okutucu-Özyurt, AND M. P. Mengüç, "Near-field radiative transfer in spectrally tunable double-layer phonon-polaritonic metamaterials," *J. Quant. Spectrosc. Radiat. Transf*, vol. 212, pp. 120–127, Jun. 2018, doi: 10.1016/j.jqsrt.2018.03.015.
[7] Fiorino et al., "A Thermal Diode Based on Nanoscale Thermal Radiation," *ACS Nano.*, vol. 12, no. 6, pp. 5774–5779, May 2018, doi: 10.1021/acsnano.8b01645.
[8] W. Zhu et al., "Quantum mechanical effects in plasmonic structures with subnanometre gaps," *Nat. Commun*, vol.7, Jun. 2016, Art. no. 11495, doi: 10.1063/1.1365944.
[9] J.-M. Nam, J.-W. Oh, H. Lee, and Y. D. Suh, "Plasmonic Nanogap-Enhanced Raman Scattering with Nanoparticles," *Acc. Chem. Res.*, vol. 49, no. 12, pp. 2746–2755, Nov. 2016, doi: 10.1021/acs.accounts.6b00409.
[10] J. Kim et al., "Single-Particle Analysis on Plasmonic Nanogap Systems for Quantitative SERS," *J. Raman Spectrosc.*, vol. 52, no. 2, pp. 375–385, Fab. 2019, doi: 10.1002/jrs.6030.
[11] S. K. Lamoreaux, "The Casimir force: background, experiments, and applications," *Rep. Prog. Phys.*, vol. 68, pp. 201–236, Nov. 2004, doi: 10.1088/0034-4885/68/1/R04.
[12] S. Sharma and M. Madou, "A new approach to gas sensing with nanotechnology," *Phil. Trans. R. Soc. A*, vol. 370, no. 1967, pp. 2448–2473, May 2021, doi: 10.1098/rsta.2011.0506.
[13] Y. Hishinuma, T. H. Geballe, B. Y. Moyzhes, and T. W. Kenny, "Refrigeration by combined tunneling and thermionic emission in vacuum: Use of nanometer scale design," *Appl. Phys. Lett.*, vol. 78, no. 17, pp. 2572–2574, Apl. 2001, doi: 10.1063/1.1365944.
[14] M. Francoeur, R. Vaillon, and M. P. Mengüç, "Thermal Impacts on the Performance of Nanoscale-Gap Thermophotovoltaic Power Generators," *IEEE Trans. Energy Convers.*, vol. 26, no. 2, pp. 34–39, Jun. 2011, doi: 10.1109/tec.2011.2118212.
[15] Y. Hishinuma, T. H. Geballe, B. Y. Moyzhes, and T. W. Kenny, "Measurements of cooling by room-temperature thermionic emission across a nanometer gap," *Appl. Phys. Lett.*, vol. 94, no. 7, pp. 4690–4696, Oct. 2003, doi: 10.1063/1.1606852.
[16] W. Li et al., "A Review of Recent Applications of Ion Beam Techniques on Nanomaterial Surface Modification: Design of Nanostructures and Energy Harvesting," *Small*, vol.15, Jun. 2019, Art. no. 1901820, doi: 10.1002/smll.201901820.
[17] B. Song et al., "Radiative heat conductances between dielectric and metallic parallel plates with nanoscale gaps," *Nat. Nanotechnol.,* vol. 11, pp. 509–514, Mar. 2016, doi: 10.1038/nnano.2016.17.
[18] A. Fiorino et al., "Nanogap near-field thermophotovoltaics," *Nat. Nanotechnol.,* vol. 13, pp. 806–811, Jun. 2018, doi: 10.1038/s41565-018-0172-5.
[19] M. Shimofuri, A. Banerjee, Y. Hirai, and T. Tsuchiya, "Observation of Pull-In by Casimir Force in MEMS-Controlled Nanogap Fabricated by Silicon Cleavage," *in IEEE MEMS,* Tokyo, Japan, 2022, pp. 511–514, doi: 10.1109/MEMS51670.2022.9699645.
[20] J. R. Kermode et al., "Low-speed fracture instabilities in a brittle crystal," *Nature,* vol. 455, pp. 1224–1227, Oct. 2008, doi: 10.1038/nature07297.
[21] A. Uesugi, Y. Hirai, K. Sugano, T. Tsuchiya, O. Tabata, "Effect of crystallographic orientation on tensile fractures of (100) and (110) silicon microstructures fabricated from silicon-on-insulator wafers," *Micro & Nano Lett.,* vol. 10, no. 12, pp. 678–682, Dec. 2015, doi: 10.1049/mnl.2015.0334.
[22] W. M. van Spengen, R. Puers, and I. De Wolf, "A physical model to predict stiction in MEMS," *J. Micromech. Microeng.*, vol. 12, no. 5, pp. 702–713, Aug. 2002.
[23] H. B. G. Casimir, "On the Attraction between Two Perfectly Conducting Plates," *Proc. Kon. Nederland. Akad. Wetensch.*, vol. 51, pp. 793–795, May 1948.
[24] E. M. Lifshitz, "The theory of molecular attractive forces between solids," *Sov. Phys. JETP,* vol. 2, no. 1, pp. 94–110, Jan. 1956, doi: 10.1016/B978-0-08-036364-6.50031-4.
[25] L. Duraffourg and P. Andreucci, "Casimir force between doped silicon slabs," *Physics Letters A,* vol. 359, no. 5, pp. 406–411, Dec. 2006, doi: 10.1016/j.physleta.2006.06.083.

Masaki Shimofuri received the B.S. and M.Eng. degrees from Kyoto University, Kyoto, Japan. He is currently pursuing the Ph.D. degree with the Department of Micro Engineering, Kyoto University. His research interests include micro/nano-electromechanical systems, MEMS transducers, and nanogap fabrication technology.

Amit Banerjee received his M.Sc. and Ph.D. degrees from Indian Institute of Technology Kanpur, India. He is currently a junior associate professor in the graduate school of engineering in Kyoto University, Japan. His research interests include Nano-mechanics and micro/nano-electromechanical systems.

Jun Hirotani (Member, IEEE) received the B.E., M.E., and Ph.D. degrees from Kyushu University, in 2009, 2011, and 2013, respectively. He became an Assistant Professor with the Department of Electrical Engineering, Nagoya University in 2015. He is currently an Associate Professor with the Department of Micro Engineering, Kyoto University, and a PRESTO researcher, Department of Strategic Basic Research, Japan Science and Technology Agency. His research interests include nanoscale energy transfer, thermophysical properties of nanomaterials, and flexible electronic and thermal devices.

Yoshikazu Hirai (Member, IEEE) received the Ph.D. degree from Kyoto University, Japan, in 2007. He was a Postdoctoral Researcher with the Graduate School of Engineering, Kyoto University. He joined the Advanced Biomedical Engineering Research Unit, Kyoto University, in 2009 and an Assistant Professor with the Department of Micro Engineering, Kyoto University, in 2013. Since 2021, he has been a Junior Associate Professor with the Department of Mechanical Engineering and Science, Kyoto University. His current research interests include Fabrication and Packaging for Generic MEMS/NEMS, Silicon/Polymer based MEMS devices and systems, Atomic MEMS devices, Micro/Nanofluidic systems for microphysiological systems. He has received several academic awards such as The Institute of Electrical Engineers of Japan (IEEJ) Distinguished Paper Award in 2017, and Outstanding Reviewer Awards in 2016 of Journal of Micromechanics and Microengineering. He is an Associate Editor of IEEE Transactions on Nanotechnology and Editorial Board Member of Sensors and Actuators Reports.

Toshiyuki Tsuchiya (Member, IEEE) received his B.S. and M.S. degree from the University of Tokyo, Japan, and his Ph.D. degrees from Nagoya University, Japan, in 1991, 1993, and 2002, respectively. He worked with Toyota Central Research and Development Laboratories from 1993 to 2004. In 2004, he joined Kyoto University as an associate professor and since 2019 he is a professor in the Department of Micro Engineering, Kyoto University, Japan. He is currently engaged in the research of silicon surface micromachining, its application in MEMS, the mechanical property evaluation of micromaterials, and the reliability of MEMS devices.

Dr. Tsuchiya was a recipient of the R&D Awards in 1997 and the IEC 1906 Award in 2012. He is a member of MRS, the Institute of Electrical Engineers of Japan, the Japan Society of Applied Physics, and the Japan Society of Mechanical Engineers.